Editors' Suggestion

Unusual pressure-induced metallic state in the correlated narrow band-gap semiconductor FeSi

G. R. Hearne,* P. Musyimi, and S. Bhattacharjee
Department of Physics, University of Johannesburg, P.O. Box 524, Auckland Park 2006, Johannesburg, South Africa

M. K. Forthaus and M. M. Abd-Elmeguid
II. Physikalisches Institut, Universität zu Köln, Zülpicher Str. 77, D-50937 Köln, Germany

(Received 14 June 2019; published 10 October 2019)

Compressing FeSi induces a progressive semiconductor to metal transition, onset at $P \geqslant 15$ GPa at temperatures below T_{max} determined by the degree of disorder in the sample. At high pressure preceding charge-gap closure, a broad maximum manifests in the $\rho(T)$ data at T_{max} and is a feature which persists into the metallic state. The extremum in $\rho(T)$ occurs at $T_{max} \sim 40$ K at ~11 GPa and shifts monotonically to ~240 K as pressure is increased to ~32 GPa, in the most detailed example of three series of measurements involving pressurized FeSi with different degrees of disorder. The transition to a metallic phase is an electronic change only, in that the B20-type crystal structure is retained up to 30 GPa, with no evidence of a discontinuity in the volume-pressure equation of state data. Samples from the same ingot subjected to different quasihydrostatic conditions reveal different values of the critical pressure of the electronic transition, its width, and pressure dependences of T_{max}. This attests to sensitivity of the electronic transition to the degree of disorder in the investigated sample. The metallic state has neither Fermi-liquid nor non-Fermi-liquid behavior. Such an unusual pressure-induced correlated metallic state in FeSi is attributed to extended states within the $3d$-$3p$ hybridization gap originating from disorder and compression tuning of the mobility edge relative to the Fermi level. The metallic state has also been investigated in external magnetic fields up to 8 T at low temperatures ($2\,\text{K} \leqslant T \leqslant 20\,\text{K}$) at 15 and 19 GPa. This reveals a positive magnetoresistance, as observed in doped $Fe_{1-x}Co_xSi$ samples at ambient pressure, suggesting that in the majority and minority spin bands there is a field-induced modification of the respective magnitudes of charge-carrier populations which have different mobilities.

DOI: 10.1103/PhysRevB.100.155118

I. INTRODUCTION

The unusual electronic and magnetic properties of narrow-band semiconductors and possibilities of exploiting these for technological applications have been the subject of extensive studies over many years [1]. Among these the correlated transition-metal monosilicide ε-FeSi has stirred considerable debate surrounding its unusual temperature-dependent properties. A small charge gap $E_g \sim 50$ meV is discerned at low temperatures but metallic behavior ensues above ~340 K, signifying that the charge gap is temperature dependent [2,3]. Magnetic susceptibility $\chi(T)$ is quenched below ~80 K, progressively rises to a broad maximum at ~500 K, and then decreases with Curie-Weiss type behavior above that temperature involving Fe magnetic moments of $\sim 2\,\mu_B$ per atom [4]. No magnetic ordering is discerned in the range 300–0.04 K [5]. These temperature-dependent properties evoked curiosity and debate already ~60 years ago [6,7], which has continued up to date [1,8–10]. Advanced electronic structure calculations show that narrow gapped behavior below room temperature (RT) stems from strong Fe-$3d$/Si-$3p$ hybridization, but electron correlations play an important role as well [10–12]. FeSi in the B20 distorted rocksalt structure fortuitously has electron correlations of an extent (Hubbard $U \sim 1$ eV and $3d$ bandwidth ~0.5 eV) that locates it near to an insulator-metal transition [12]. This entails a quasiparticle feature involving highly peaked density of states (DOS) at the Fermi level E_F, flanked by upper and lower Hubbard subbands (satellites) at $\pm U/2$ [13]. Crucially, Fe-$3d$/Si-$3p$ hybridization has both screened the on-site repulsion U down to ~1 eV and opens a narrow gap in the quasiparticle peak, with consequent high-DOS features at gap edges [12,14]. Earlier electronic structure measurements confirm this narrow peaked DOS near E_F [15–17]. Thus hybridization and electron correlations account for a small E_g, renormalized peaked DOS at charge-gap edges, and above-mentioned temperature dependence of E_g and $\chi(T)$ [10,12].

In this context, pressurization is expected to generate well-defined changes of hybridization and correlations in FeSi until gap closure occurs and thereby likely induces an unusual metallic state [10], different from those reported in various doping studies [3,18–21]. Studies of FeSi under pressure have indeed been attempted previously [22–24], although limited to ~10 GPa where gap closure and metallization was not attained. We have both extended such temperature-dependent electrical resistivity $\rho(T)$ investigations and monitored the structural response by energy-dispersive x-ray diffraction (ED-XRD) at RT to 30–35 GPa. We demonstrate that an unusual metal state ensues, beyond previous ~10-GPa investigation limits, and this does not involve any structural instability of the original noncentrosymmetric cubic B20-type structure.

*Corresponding author: grhearne@uj.ac.za

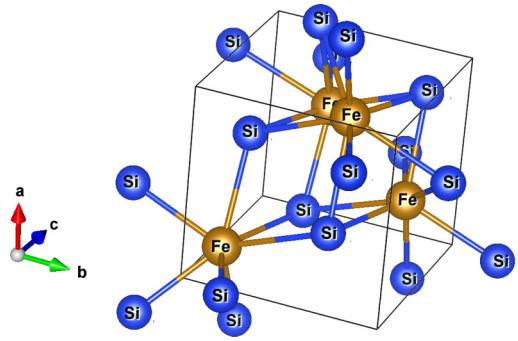

FIG. 1. Crystal structure of ε-FeSi, showing the B20-type cubic unit cell with four formula units. Each Fe atom has a sevenfold coordination of Si atoms involving three sets of Fe–Si near-neighbor bond lengths [26].

In ε-FeSi (space group $P2_13$, $Z = 4$, lattice parameter $a = 4.489$ Å), each Fe atom has a sevenfold coordination of Si with three different sets of Fe–Si bond lengths [25,26] (see Fig. 1) compared with six Si neighbors at equal distances in the underlying rocksalt structure. Details of how the distorted rocksalt B20-type structure relates to or is derived from the simplest binary cubic NaCl and CsCl structures are provided in Ref. [26].

II. EXPERIMENTAL

Sample stoichiometry is reflected in the residual resistivity ratio (RRR), i.e., $\rho(300\,\mathrm{K})/\rho(4\,\mathrm{K})$, used as a figure of merit in evaluating sample quality. The original polycrystalline ingot used in this study had RRR∼14 000 (see Fig. 2), comparable to quality stoichiometric samples of previous studies [24,27,28]. Details of sample preparation are in Ref. [18]. A fragment of the original synthesized ingot was ground into powder. Representative XRD patterns show all indexed reflections correspond to the B20 structure with no indication of parasitic phases. Such structural and other physical characterizations at ambient pressure are in Sec. S1 of the Supplemental Material [29–31].

Powdered sample was loaded into cavities in gasketed diamond-anvil cells (DACs), appropriately prepared for resistivity pressure studies and separate ED-XRD pressure measurements.

A. Methodology of electrical resistance measurements under pressure

Three series of measurements were conducted on powdered samples derived from the same original polycrystalline ingot of FeSi synthesized as indicated in Ref. [18]. These three runs involved powdered samples subjected to different degrees and durations of grinding in a pestle and mortar. Pressurization involved different degrees of deviation from hydrostaticity depending on the DAC preparation procedures used. The powdered samples and the corresponding series of measurements were designated as FeSi-UK, FeSi-UJ#1, and FeSi-UJ#2. These different powder preparation conditions and levels of quasihydrostaticity are expected to render different residual stress states, corresponding to a distribution

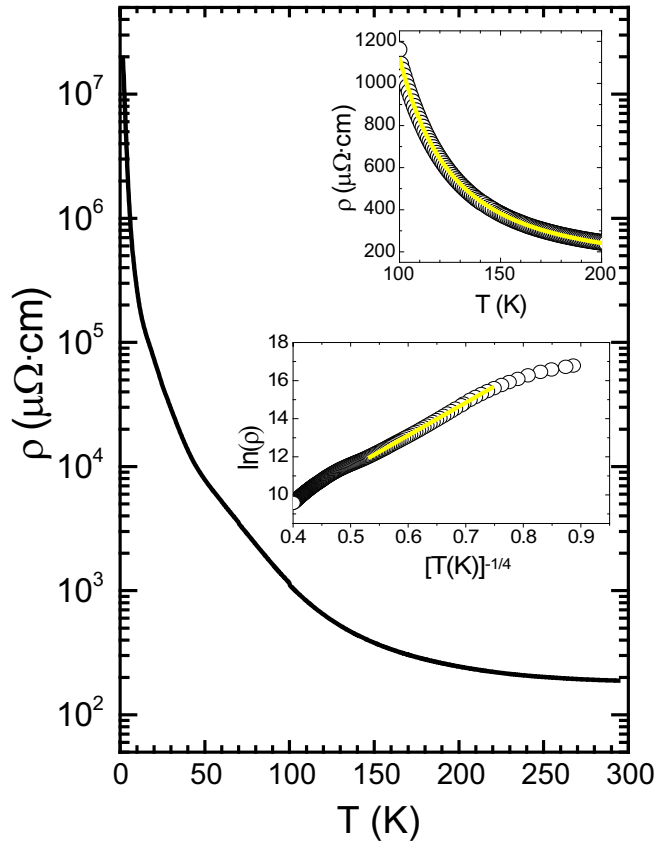

FIG. 2. Temperature dependence of the resistivity in the range 300–2 K of the FeSi sample [28], which involved a DC four-probe measurement at ambient pressure on a bar cut from the original polycrystalline ingot. Top inset shows data in the 200–100 K regime and solid line fit involving Arrhenius thermally activated behavior $\rho \propto \exp(E_g/2k_BT)$, where $E_g = 63$ meV is the derived charge gap. Bottom inset is a linearized plot of the variable range-hopping formulation $\rho \propto \exp[(T_0/T)^{1/4}]$, where the solid line is a linear fit in the range 20–4 K to yield a Mott temperature $T_0 = 1.1 \times 10^5$ K. The residual resisitivty ratio $\rho(4.2\,\mathrm{K})/\rho(300\,\mathrm{K}) \approx 14\,000$ [24].

of strain fields and distribution of defects in the three samples, although no attempt was made to quantitatively assess this in detail.

Powdered sample FeSi-UK involved extensive grinding i.e., several repeated grindings for several minutes under acetone, to a fine powder before loading into a nonmetallic gasket described below. FeSi-UJ#1 also involved extensive grinding to a powder compared with FeSi-UJ#2 which involved much more limited grinding of a fragment to a powder. In both of these latter cases, UJ#1 and UJ#2, the powdered sample was loaded into the cavities of insulated metallic gaskets for separate $\rho(T)$ runs of DACs configured as described below.

The FeSi-UK pressurization involved a low thermal expansion Ti-alloy Merrill-Basset-type DAC with diamond anvils having culet diameters of 600 μm. The nonmetallic gasket was prepared from a hardened mixture of Al_2O_3 powder and Stycast-1266 epoxy, preindented to a thickness of ∼60 μm. A cavity of ϕ≈200 μm was drilled in the center of the indentation into which the powdered sample was loaded for

pressurization. All of this is similar to our previous resistivity pressure studies of Co-doped FeSi [32]. Such a gasket is easier to prepare than an insulated metal-foil version normally used for such DAC resistivity pressure studies. There is also no risk of short-circuit of the Au or Pt electrodes to a metallic gasket substrate from cut through at very high compression. Moreover, such a nonmagnetic DAC was suitable for magnetoresistance measurements at selected high pressures.

For the separate runs involving FeSi-UJ#1 and FeSi-UJ#2 diamond anvils with culet diameters of 550 μm beveled to 650 μm were mounted in Inconel-718 MB-DACs. Inconel-750 metal foil was used as the confining gasket. Starting from a thickness of 200 μm this was preindented down to a final thickness of 40–50 μm. One side of the indented region was first insulated by coating on a mixture of Al_2O_3 powder and Stycast-1266 epoxy. This was pressed into the indented region and surrounding area, as well as into the previously drilled cavity. A microdrill of 100-μm diameter was used to drill and enlarge a 130-μm-diameter hole, constituting an insulated sample chamber at the center of the preindentation.

A DC four-probe method was used for resistance measurements $R(T)$, involving a current-reversal technique to eliminate thermoelectric voltages generated at various junctions in the leads. Au or Pt electrodes were configured into the microscopic sample cavity of the insulated gasket and pressed into contact with the sample powder upon pressurization.

For all three resistivity runs no liquid pressure-transmitting medium was used to avoid having an insulating barrier infiltrate between electrode and sample. The insulating epoxy ring surrounding the sample is considered to act as a pressure-transmitting medium. Two or three ruby balls were embedded in the sample powder between the voltage leads spaced $\sim$50 μm apart, for pressure determination from the ruby R_1 line fluorescence at room temperature [33]. Temperature-dependent resistance (R-T) data to $\sim$35 GPa have been obtained by cycling to 3 K in a home-developed electrical-transport station customized for the DAC, with a Si diode in close proximity to determine temperature of the sample. These resistance data were converted to estimates of resistivity (ρ-T) from sample and electrode geometry.

At low pressures $P \leqslant 3$ GPa the Inconel-718 DAC with metallic gaskets tended to show changes of up to $\sim$1 GPa upon temperature cycling. So, for R-T runs involving UJ#1 and UJ#2, only data above $\sim$4 GPa were used for analysis where temperature-induced changes in pressure were well below 1 GPa.

The average pressure from the two or three ruby balls was taken as the set pressure value. There is definitive line broadening of these fluorescence bands due to deviations from ideal hydrostaticity for pressures exceeding several GPa [34]. The R_1 and R_2 fluorescence peaks remained resolved up to the highest pressure. As expected, this resolution progressively deteriorated upon increasing pressure up to the highest values attained at 30–35 GPa and this progression differed for the three runs. No attempt was made to quantitatively assess the deviation from hydrostatic behavior from the peak broadening for the three runs on the samples described above.

B. ED-XRD measurements under pressure

Structural parameters of the FeSi-UK sample as a function of pressure were obtained from ED-XRD measurements at room temperature for pressures up to 30 GPa. These measurements were conducted at the beamline F3 of HASYLAB, Hamburg, Germany. The x-ray beam was collimated to dimensions of $100 \times 100\,\mu m^2$ after entering the experimental hutch. The Ge detector was mounted at a fixed 2θ angle with respect to the incident beam such that

$$E d_{hkl} = \frac{hc}{2\sin\theta} = \frac{6.199}{\sin\theta}\text{keV Å} = 72.933\,\text{keV Å}, \quad (1)$$

for the reflection at energy E satisfying Bragg's law for the separation between (h, k, l) planes d_{hkl}.

Pressure was generated using a miniature Merrill-Basset type DAC equipped with anvils of the conical Boehler-Almax design with culet diameters of 600 μm. An Inconel-750 gasket with an initial thickness of 200 μm was preindented to a thickness of 50–60 μm and a sample chamber of 200-μm diameter drilled in the center of the indentation.

Powdered sample derived from grinding a fragment of the original ingot was loaded into the gasket cavity to fill it to $\sim$2/3 of its full capacity. Some ruby chips were also loaded into the cavity for pressure determination by way of the ruby R_1 line fluorescence [33]. An ED-XRD measurement was recorded at ambient pressure upon closure of the DAC without pressurization. Liquid nitrogen as pressure-transmitting medium was then loaded into the cavity and the DAC closed to an initial pressure of $\sim$1 GPa for subsequent XRD measurements at pressure.

The spectra were analyzed using the program EDXPOWD 3.13 which was specially developed by F. Porsch (RTI GmbH Paderborn, Germany, 1996) for high-pressure x-ray diffraction using the DAC.

III. RESULTS AND DISCUSSION

A. Pressure-induced semiconductor to metal transition

Figure 3 depicts $\rho(T)$ measurements of sample powder designated FeSi-UK, for pressures up to $\sim$32 GPa. This is the most detailed series of measurements of the three separate runs on powdered samples derived from the same synthesized ingot. Each powdered sample in these runs has been subjected to different degrees of grinding prior to loading in the DAC and different quasihydrostatic conditions dependent on DAC preparation procedures. Section S2 of the Supplemental Material [29] includes selected results of the other two runs on samples designated FeSi-UJ#1 and FeSi-UJ#2.

Sample FeSi-UK in Fig. 3 at $P < 10$ GPa has $\rho(T)$ behavior similar to previous resistivity pressure studies [19,22–24]. The ρ(294 K)$\sim$179 $\mu\Omega$ cm value at 1.6 GPa accords with FeSi resistivity measurements at ambient conditions [24,27]. In the low-pressure regime up to $\sim$6.5 GPa the RT resistivity, ρ(294 K), has a comparatively stronger pressure dependence than at higher pressures. This is also seen in the other runs, for example, FeSi-UJ#2 in Fig. S6 of the Supplemental Material [29], and is typical of the initial evolution of charge-gap closure and related RT resistivity behavior in semiconductors under pressure [24,32].

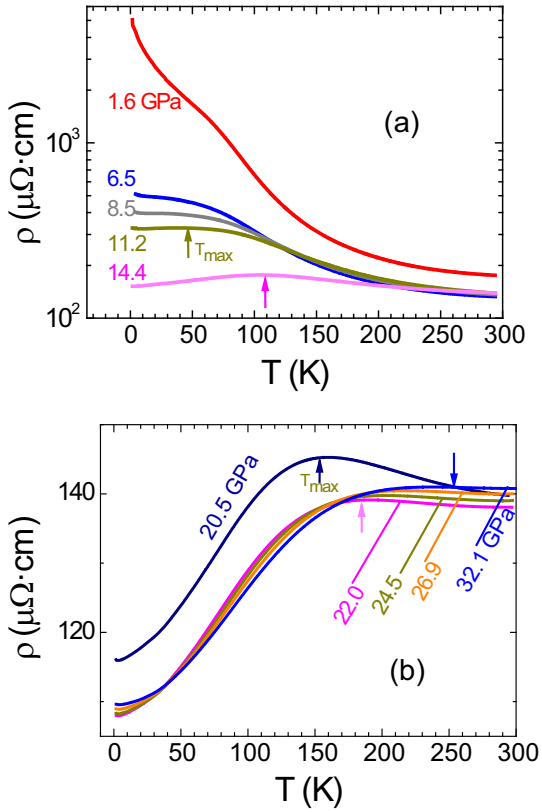

FIG. 3. (a) Temperature dependence of resistivity of sample FeSi-UK up to maximum pressurization of 32.1 GPa. Resistivity curves below 11.2 GPa have $d\rho/dT < 0$. (b) Temperature dependence of resistivity in the HP metallic electronic phase at $P >$ 15 GPa, where the charge gap $E_g \approx 0$, exemplifying a broad maximum at T_{max} delineated by arrows in some curves.

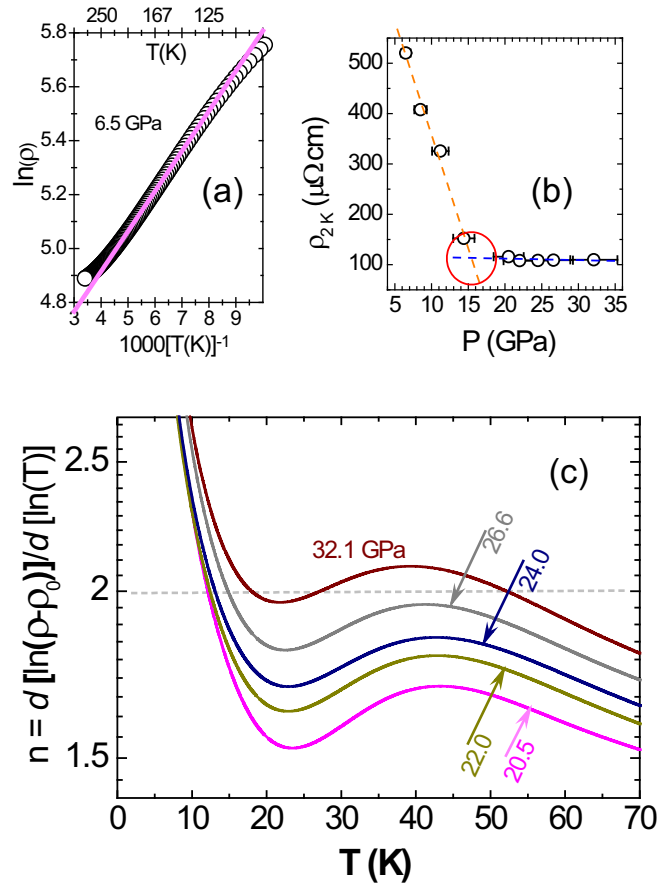

FIG. 4. (a) Example of extraction of E_g at 6.5 GPa of the LP phase of sample FeSi-UK, from a linear fit (solid line) to the high-temperature data range 150–200 K assuming activated hopping transport $\ln \rho = \frac{E_g}{2k_B T} + \text{const}$. (b) Evolution of LT resistivity $\rho(2\ K)$ to identify the semiconductor→metal transition. (c) Analysis of HP data of metallic behavior of sample FeSi-UK, using a power-law formulation $\rho(T) = \rho_0 + AT^n$. Derivative $d[\ln(\rho(T) - \rho_0)]/d(\ln T)$ provides the exponent n at any LT [36]. There is no extended LT range as $T \to 0$ K where either Fermi-liquid behavior ($n = 2$) or non-Fermi-liquid characteristics ($1 \leqslant n \leqslant 1.5$) are exhibited.

Up to ∼8.5 GPa, FeSi-UK displays semiconducting behavior evidenced by a negative temperature coefficient of resistivity, $d\rho/dT<0$, throughout the temperature range 300–2 K [see Fig. 3(a)]. The charge gap E_g is extracted from the slope of $\ln[\rho(T)]$ vs $1000T^{-1}$ Arrhenius plots in the range 150–200 K; for example see Fig. 4(a). E_g values start at ∼50 meV at ∼1.6 GPa, consistent with those reported in similar work at low pressures [22–24].

Figure 3(a) shows that at ∼8.5 GPa, resistivity values start to plateau at low temperatures (LT) $T<50$ K. At the next highest pressure 11.2 GPa and beyond, $\rho(T)$ curves exhibit a broad maximum at a temperature T_{max} where $d\rho/dT>0$ metallic-like signatures occur below this temperature (see Fig. 3). The extremum at T_{max} is pressure dependent and above T_{max} there is $d\rho/dT<0$ behavior, characteristic of carrier excitation across a small energy gap.

Whereas LT resistivity values at 2 K show a relatively strong pressure dependence up to ∼15 GPa, they plateau at ∼110 $\mu\Omega$ cm beyond this pressure and E_g extrapolates to zero by ∼15 GPa; see Fig. 4(b) and Fig. 5(a), respectively. This signals that a high-pressure (HP) metallic majority phase is stabilized at ∼15 GPa. Even at $P>15$ GPa in the HP metallic phase, $\rho(T)$ data continue to exhibit an extremum at T_{max} which shifts monotonically from ∼40 K at ∼11 GPa to ∼240 K at ∼32 GPa; see Figs. 3(b) and 5(a). Similar qualitative behavior is seen in the two additional experiments on samples FeSi-UJ#1 and FeSi-UJ#2; see Sec. S2 of the Supplemental Material [29]. The behavior of E_g and T_{max} for the three cases in Figs. 5(a) and 5(b) is therefore supposed to involve different degrees of disorder (e.g., distribution of strain fields and defects) and this shifts the LP-semiconducting→HP-metallic transition pressure to different values, as will be discussed later in the text.

To further probe the nature of the HP metallic ground state in FeSi-UK an analysis in terms of power-law behavior $\rho(T) = \rho_0 + AT^n$ at LT (involving residual resistivity ρ_0 and effective scattering cross-section A constants at each pressure) was effected [35,36]. Figure 4(c) presents at each pressure deduced values of n as a function of temperature. It demonstrates there is no extended LT range where either Fermi-liquid behavior ($n = 2$) or non-Fermi-liquid (NFL) behavior ($1 \leqslant n \leqslant 1.5$) is prevalent as $T \to 0$ K [36], in contrast to $n = 1$ NFL behavior observed for the pressure-induced

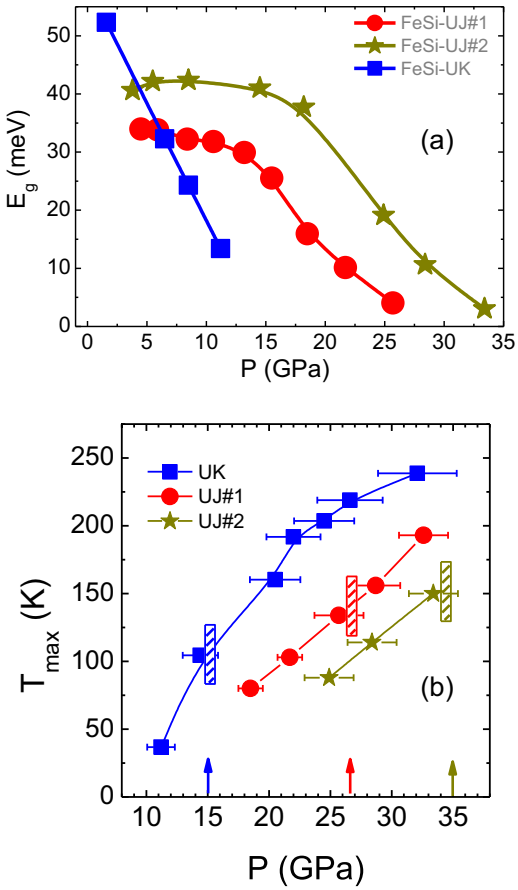

FIG. 5. (a) Comparison of the trend of E_g for the three series of measurements on samples derived from the same synthesized ingot, subjected to both different degrees of grinding prior to loading in the DAC and hydrostaticity under pressure. Solid lines guide the eye. (b) Pressure evolution of the extremum T_{max} in $\rho(T)$ data (e.g., Fig. 3) for the three series of measurements. Vertical error bars for T_{max} are the size of the symbols. Arrows on the horizontal axis and hatched bars indicate pressures where E_g extrapolates to zero (see top panel) and beyond which the HP metallic electronic phase is stabilized. Solid lines guide the eye.

quantum-phase transitions of $Fe_{1-x}Co_xSi$ at low doping concentrations of Co [32].

B. Pressure response of the B20 structure

To check whether the pressure-induced semiconductor to metal transition is connected to a structural phase transition, the lattice response of the B20-type structure to compression has been considered. Representative ED-XRD patterns recorded at pressures to 30 GPa at RT are shown in Fig. 6(a). At each pressure all main peaks can be indexed according to the cubic B20-type structure. Relative intensities differ between spectra due to texture effects in the small sample volume in combination with a probing beam size of $100 \times 100\,\mu m^2$ and do not reflect the atomic arrangement. So, although Rietveld refinements are not possible to determine atomic positions, lattice parameters were extracted using (110), (111), (210), (211), and (321) reflections from the cubic unit cell.

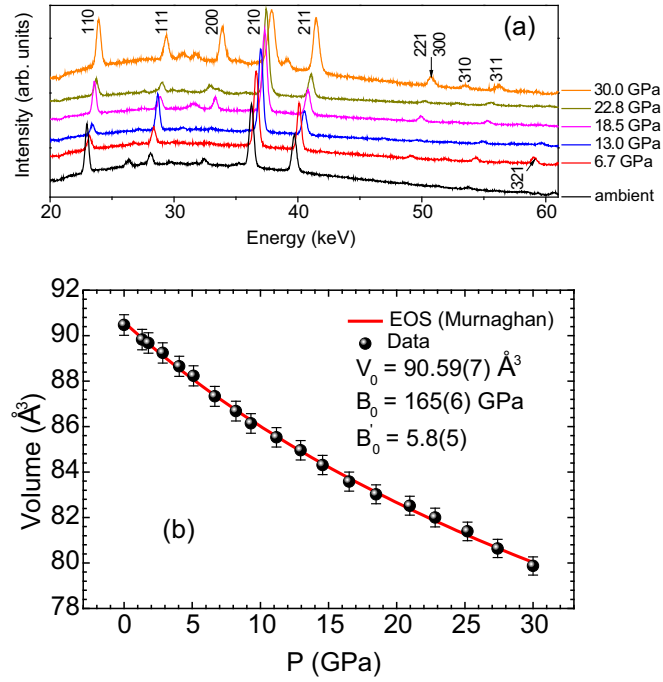

FIG. 6. (a) Representative selection of ED-XRD patterns of sample FeSi-UK measured up to 30 GPa at RT. Peaks not indexed are from fluorescence events in the detector or solidified nitrogen pressure-transmitting medium. (b) Corresponding unit-cell volume behavior of the B20 lattice structure retained throughout the pressure range. Solid line through data points is the Murnaghan equation of state.

The deduced unit-cell volume versus pressure presented in Fig. 6(b) shows no discontinuous change up to 30 GPa. The derived unit-cell volume as a function of pressure in Fig. 6(b) was fitted with the Murnaghan equation of state (EOS) [37], to obtain the indicated parameters $V_0 = 90.6(1)\,Å^3$, $B_0 = 167(7)$ GPa, and $B_0' = 5.6(5)$. If B_0' is fixed at 4 then the Murnaghan EOS yields $B_0 = 188(2)$ GPa. These values of B_0 are closely compatible with that derived from ED-XRD pressure measurements by Lin *et al.* [38] and the values from references cited therein, where B_0 falls mainly in the range 185–160 GPa. This includes a variety of measurements involving single-crystal XRD, powder XRD, neutron diffraction, and ultrasonic spectroscopy at ambient pressure. No structural transition or discontinuity in the EOS is discerned, in some of these cases to well beyond 30 GPa.

We conclude that in our FeSi sample there is no indication of a structural phase transition of the cubic B20-type lattice when there is an electronic transition from LP semiconductor to HP metal beyond ∼15 GPa.

C. Rationalizing the driving mechanism of the semiconductor-metal transition

This unusual HP metallic state emanated from the corresponding intriguing LP semiconductor state is rationalized as follows. In the LP semiconducting phase disorder from crystal lattice heterogeneities (e.g., chemical disorder or distribution of strain fields) introduces band-edge tails extending into the hybridization gap prevalent without disorder

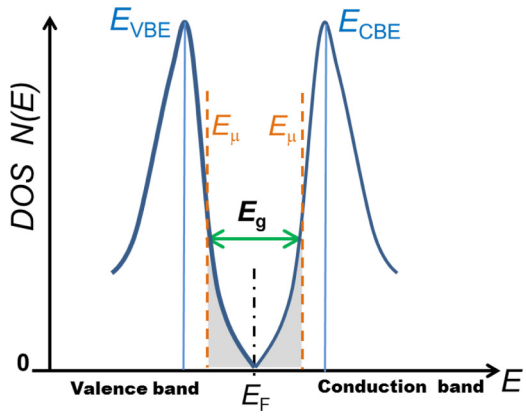

FIG. 7. Schematic DOS of FeSi near the Fermi level E_F at ambient conditions. Mobility edges E_μ arising from crystal lattice heterogeneity (i.e., disorder) separate the localized (shaded) states from extended states in band-edge tails in the region E_{VBE} to E_{CBE} [24,39]. This demonstrates how the gap E_g is manifest in the DOS.

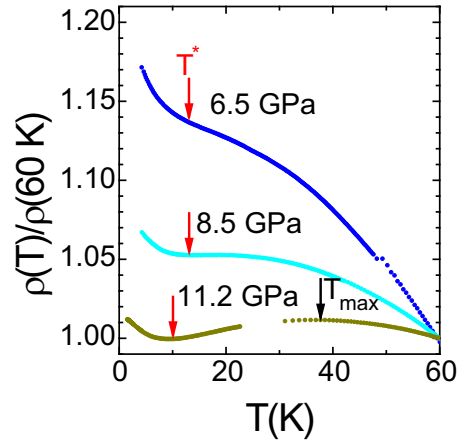

FIG. 8. Temperature dependence of the normalized resistivity $\rho(T)/\rho(60\,\mathrm{K})$ for $6.5\,\mathrm{GPa} \leqslant P \leqslant 11.2\,\mathrm{GPa}$ at low temperatures ($\rho < 60\,\mathrm{K}$). Red arrow marks a kink/upturn in $\rho(T)$ at $T^* \sim 12\,\mathrm{K}$; black arrow marks the maximum in $\rho(T)$ for 11.2 GPa at ~38 K.

$|E_{VBE} - E_{CBE}|$, involving edges of the valence band (VBE) and conduction band (CBE) depicted in Fig. 7 [24,39]. VBE and CBE each have a comparatively high DOS arising from the $3d$-$3p$ hybridization and electron correlations [10,12,14]. A mobility edge E_μ separates extended from localized states within band-edge tails. Moreover, electron conduction is through activation across the charge gap $E_g \sim 2|E_F - E_\mu| \leqslant |E_{VBE} - E_{CBE}|$, responsible for semiconducting behavior at $100\,\mathrm{K} < T < 200\,\mathrm{K}$ in the LP regime [Fig. 2 (top inset) and Fig. 4(a)]. The localized defect states within the gap manifest as a variable range-hopping conductivity mechanism at low temperatures $T < 40\,\mathrm{K}$ at ambient pressure [24]; see Fig. 2 (bottom inset).

The DOS profile in the region E_{VBE} to E_{CBE} and position of E_μ relative to E_F depend on the degree of lattice heterogeneity, i.e., disorder, whatever its origin [39,40]. A reduction in unit-cell volume through pressurization broadens band edges and associated disorder-induced tails (see Fig. 7) and shifts E_μ towards E_F, thus decreasing E_g. This pressure-driven evolution of E_μ towards E_F eventually results in a finite low density of extended states at E_F. A resultant HP electronic phase occurs with metallic signatures $d\rho(T)/\mathrm{d}T > 0$ at LT involving comparatively high $\sim 10^2\,\mu\Omega\,\mathrm{cm}$ "bad metal" resistivity values at RT; see Fig. 3. The characteristic temperature T_{max} in Figs. 3(b) and 5(b) is determined by the magnitude of extended DOS at E_F, in turn governed by degree of disorder in the sample at a certain pressure. Thus, T_{max} is an energy scale related to degree of disorder in the sample. Above T_{max} thermal energy input k_BT of several meV is sufficient to excite electrons from the peaked DOS at E_{VBE} to unoccupied states above E_F. This then becomes the dominating mechanism of charge-carrier generation and a consequent $d\rho(T)/dT<0$ semiconductinglike signature.

As $E_g \to 0$ with increasing pressure the DOS initially developed at E_F is much smaller than at band edges E_{VBE} and E_{CBE}, depicted in Fig. 7. Continued pressurization further broadens bands and smears band-edge tails from disorder due to a distribution of strain values from deviations of hydrostaticity. Consequently the DOS at E_F increases, effectively extending the LT range over which metallic $d\rho(T)/dT>0$ signatures occur. The DOS also decreases at band edges E_{VBE} and E_{CBE}. Hence T_{max} will be at higher temperatures with increasing pressure, corresponding to where electron activation from E_{VBE} to above E_F becomes the dominant charge-carrier mechanism and $d\rho(T)/dT<0$, in agreement with experimental observations of Fig. 5(b).

D. Nature and elaboration of the HP metallic phase

To elucidate the nature of the HP metallic state, the low-temperature part of $\rho(T)$ of FeSi-UK and its change with pressure and external field is considered here. Particularly interesting is the temperature dependence of the resistivity of FeSi-UK at low temperatures for $6.5\,\mathrm{GPa} \leqslant P \leqslant 11.2\,\mathrm{GPa}$. In this pressure regime at $T \leqslant 60$ K the resistivity has a much weaker temperature dependence than curves at $P < 6.5$ GPa; see Figs. 2 and 3(a). So, in Fig. 8 we rather depict the electrical resistivity normalized to its value at 60 K for $T \leqslant 60$ K in the pressure regime $6.5\,\mathrm{GPa} \leqslant P \leqslant 11.2$ GPa. The temperature dependence of $\rho(T)$ at 6.5 and 8.5 GPa shows an inflection at $T^* \sim 12\,\mathrm{K}$, which becomes more pronounced with increasing pressure and results in a minimum in $\rho(T)$ at 11.2 GPa. At 11.2 GPa $\rho(T)$ additionally reveals a maximum at $T_{max} \sim 38\,\mathrm{K}$, the origin of which was discussed in Sec. III C. Thus, starting at low temperatures the electrical resistivity for 11.2 GPa decreases with increasing temperature before passing through a local minimum at ~9 K. For temperatures $9\,\mathrm{K} < T < 38\,\mathrm{K}$ $\rho(T)$ increases with increasing temperature. At $T_{max} \sim 38\,\mathrm{K}$ the temperature coefficient again changes sign and remains negative up to room temperature. Indications of the LT inflections in $\rho(T)$ at T^* before transitioning to a HP metallic phase are also seen in the other series of measurements on FeSi-UJ#1 and FeSi-UJ#2 in the Supplemental Material, Sec. S2 [29]. But, these occur in different pressure ranges compared to FeSi-UK, likely related to the different transition pressures to the HP metallic state in Fig. 5, discussed in Sec. III A.

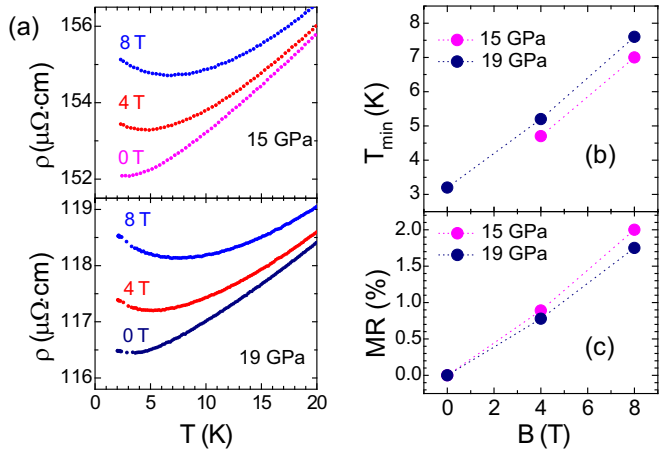

FIG. 9. (a) Temperature dependence of the electrical resistivity for $2\,\mathrm{K} \leqslant T \leqslant 20\,\mathrm{K}$ in various magnetic fields beyond the onset pressure to the metallic state ($E_g \sim 0$) for FeSi-UK at 15 and 19 GPa. (b) Magnetic-field dependence of the temperature T_{min} where a minimum in the electrical resistivity is observed at LT in (a), and (c) the magnetoresistance at 4 and 8 T.

The temperature dependence of the electrical resistivity of FeSi-UK in this pressure region, particularly at 11.2 GPa, is strikingly similar to that of the doped magnetic compounds $Fe_{1-x}Co_xSi$ with $x = 0.1$ and $x = 0.2$ at ambient pressure, where both a maximum at high temperatures and an inflection at low temperatures are observed in $\rho(T)$ [18,41]. Since an inflection in $\rho(T)$ at T^* in $Fe_{1-x}Co_xSi$ has been demonstrated to be connected with the onset of ferromagnetic order, it is supposed that in FeSi in the pressure range $6.5\,\mathrm{GPa} \leqslant P \leqslant 11.2\,\mathrm{GPa}$ magnetic ordering is onset at T^* as well.

Our investigation of the response of the electrical resistivity to external magnetic fields at LT, described in what follows, supports the suggestion that magnetic ordering occurs at LT and provides further interesting aspects of the HP metallic state. The data shown in Fig. 9 were taken in a ^{4}He flow cryostat with $2\,\mathrm{K} \leqslant T \leqslant 300\,\mathrm{K}$ and $0\,\mathrm{T} \leqslant B \leqslant 8\,\mathrm{T}$ in the pressure-induced metallic phase of FeSi at 15 and 19 GPa.

In the LT region a positive magnetoresistance (MR) is observed while the resistivity at high temperatures is not affected much. The sign of the positive MR rules out the existence of spin fluctuations but suggests a band mechanism as proposed by Onose *et al.* [41] for the positive MR observed in doped ferromagnetic $Fe_{1-x}Co_xSi$. At 15 GPa and 2 K the resistivity ρ(2 K) increases by ∼2% from ρ(2 K, 0 T)∼152 $\mu\Omega$ cm to ρ(2 K, 8 T)∼155 $\mu\Omega$ cm, as depicted in Fig. 9. There is a minimum observable in finite fields which is shifted from $T_{min}(4\,\mathrm{T}) = 4.6\,\mathrm{K}$ to $T_{min}(8\,\mathrm{T}) = 7\,\mathrm{K}$ and is apparently not visible in the zero-field measurement down to 2 K. In contrast, the temperature dependence of FeSi at 19 GPa reveals a minimum at 3.2 K in zero field already, which is shifted up to 7.6 K by application of an external field of 8 T. The MR is ∼1.7% at 2 K and 8 T and is slightly lower than that at 15 GPa. Note that the MR of FeSi both at 15 and 19 GPa is significantly lower (by a factor of 5–10) than that observed in the regime of low Co-doping-induced ferromagnetism in $Fe_{1-x}Co_xSi$ samples ($x = 0.1$ and 0.2) at ambient pressure [18,41]. This suggests that the magnitude of the field-induced magnetic moments in the high-pressure metallic state is much smaller than that reported for the Co-doped samples.

Onose *et al.* [41] have attributed the positive MR in the Co-doped samples to magnetic-field-induced adjustment of the imbalance of spin populations in the majority and minority spin bands. Carriers in opposing spin bands have different mobilities [42]. The effect of applied magnetic field is to increase the majority spin population of carriers having comparatively lower mobilities than carriers in the minority spin band, leading to an increase in resistance and consequent positive MR. By comparison with the MR values of the Co-doped samples $Fe_{1-x}Co_xSi$ [18,41], it is inferred that pressure in pristine FeSi has induced much smaller moments ($<0.2\,\mu_B$). A further inference is that applied magnetic fields in metallic FeSi at high pressure have the same effect as in $Fe_{1-x}Co_xSi$ at ambient pressure, by adjusting majority and minority spin populations involving different carrier mobilities in opposing spin bands, thus leading to a positive albeit smaller MR.

IV. CONCLUSIONS

In FeSi with a B20 distorted rocksalt-type structure, $3d$-$3p$ hybridization and the extent of electron correlations introduces an ∼50-meV gap into a very narrow quasiparticle peak at E_F. A narrow-gapped semiconductor with highly peaked DOS features at the gap edges ensues, of technological importance for premier thermoelectric materials. We have shown that pressurization induces an electronic LP-semiconducting→HP-metal transition at $P \geqslant 15$ GPa which does not involve a structural phase change, but is dependent on disorder in the lattice. Different quasihydrostatic conditions in three series investigated here lead to varying degrees of disorder. Corresponding variations occur in both the profile of in-gap states and where the mobility edge locates relative to E_F. Hence for the three cases there are different transition pressures to the HP metallic state and different behaviors of the broad extremum in $\rho(T)$ arising from in-gap states from disorder and the peaked DOS at band edges.

Normally in tuning electron correlations by pressure, spectral weight transfers from the $\pm U/2$ Hubbard satellites to a quasiparticle DOS at E_F and heavy charge carriers emerge. Our investigations infer that in FeSi having a narrow gap embedded in the quasiparticle DOS, disorder coupled to pressure plays a crucial role in the evolution of in-gap states at E_F. This leads to a correlated metallic state which has neither Fermi-liquid nor non-Fermi-liquid behavior, originating from the inhomogeneous character of combined extended defect states and $3d$-influenced DOS features evolved under pressure near E_F.

The most detailed measurements of FeSi involving one of the three series investigated here also reveals that at ∼6.5 GPa and higher, the temperature dependence of the resistivity exhibits an inflection at low temperatures $T^* \sim 12\,\mathrm{K}$. This is similar to features seen near the onset of magnetic ordering in Co doping at low concentrations in FeSi at ambient pressure. Hence it is inferred that pressure-induced magnetic ordering occurs at T^*, which in this series of measurements in the high-pressure metallic phase beyond 15 GPa becomes manifest as a minimum in the resisitivty at ∼3 K. There is also a positive magnetoresistance discerned for this putative

magnetic transition in metallic FeSi, in accord with what is seen in Co-doped FeSi samples at ambient pressure. The applied magnetic field adjusts majority and minority spin populations, which have different charge-carrier mobilities in these opposing spin bands. In pressure-induced metallic FeSi the magnetic-field-driven enhancement of the majority spin population with comparatively lower charge-carrier mobilities accounts for the positive magnetoresistance in analogy to the scenario rationalized for Co-doped FeSi at ambient pressure.

ACKNOWLEDGMENTS

N. Manyala is acknowledged for provision of the FeSi sample. G.R.H. and S.B. acknowledge financial support from the National Research Foundation of South Africa (Grant No. 105870 and for a postdoctoral research fellowship award). M.A.A. thanks E. Bauer, Vienna University of Technology, and T. Koethe, University of Cologne, for fruitful discussions.

[1] J. M. Tomczak, Thermoelectricity in correlated narrow-gap semiconductors, J. Phys.: Condens. Matter **30**, 183001 (2018).

[2] R. Wolfe, J. H. Wernick, and S. E. Haszko, Thermoelectric properties of FeSi, Phys. Lett. **19**, 449 (1965).

[3] J. F. DiTusa, K. Friemelt, E. Bucher, G. Aeppli, and A. P. Ramirez, Metal-Insulator Transition in the Kondo Insulator FeSi and Classic Semiconductors Are Similar, Phys. Rev. Lett. **78**, 2831 (1997).

[4] S. Takagi, H. Yasuoka, S. Ogawa, and J. H. Wernick, ^{29}Si NMR studies of an "unusual" paramagnet FeSi -Anderson localized state model-, J. Phys. Soc. Jpn. **50**, 2539 (1981).

[5] M. B. Hunt, M. A. Chernikov, E. Felder, H. R. Ott, Z. Fisk, and P. Canfield, Low-temperature magnetic, thermal, and transport properties of FeSi, Phys. Rev. B **50**, 14933 (1994).

[6] V. Jaccarino, G. K. Wertheim, J. H. Wernick, I. R. Walker, and S. Araje, Paramagnetic excited state of FeSi, Phys. Rev. **160**, 476 (1967).

[7] G. K. Wertheim, V. Jaccarino, J. H. Wernick, J. A. Seitchik, H. J. Williams, and R. C. Sherwood, Unusual electronic properties of FeSi, Phys. Lett. **18**, 89 (1965).

[8] A. A. Povzner, A. G. Volkov, and T. A. Nogovitsyna, Effect of pd-hybridization in strongly correlated insulator FeSi, J. Magn. Magn. Mater. **409**, 1 (2016).

[9] S. Krannich, Y. Sidis, D. Lamago, R. Heid, J.-M. Mignot, H. V. Löhneysen, A. Ivanov, P. Steffens, T. Keller, L. Wang *et al.*, Magnetic moments induce strong phonon renormalization in FeSi, Nat. Commun. **6**, 8961 (2015).

[10] J. M. Tomczak, K. Haule, and G. Kotliar, Signature of correlation effects in iron silicide, Proc. Natl. Acad. Sci. USA **109**, 3243 (2012).

[11] G. Aeppli and Z. Fisk, Kondo insulators, Comments Condens. Matter Phys. **16**, 155 (1992).

[12] V. V. Mazurenko, A. O. Shorikov, A. V. Lukoyanov, K. Kharlov, E. Gorelov, A. I. Lichtenstein, and V. I. Anisimov, Metal-insulator transitions and magnetism in correlated band insulators: FeSi and $Fe_{1-x}Co_xSi$, Phys. Rev. B **81**, 125131 (2010).

[13] M. Sentef, J. Kuneš, P. Werner, and A. P. Kampf, Correlations in a band insulator, Phys. Rev. B **80**, 155116 (2009).

[14] J. Kuneš and V. I. Anisimov, Temperature-dependent correlations in covalent insulators: Dynamical mean-field approximation, Phys. Rev. B **78**, 033109 (2008).

[15] C.-H. Park, Z.-X. Shen, A. G. Loeser, D. S. Dessau, D. G. Mandrus, A. Migliori, J. L. Sarrao, and Z. Fisk, Direct observation of a narrow band near the gap edge of FeSi, Phys. Rev. B **52**, R16981(R) (1995).

[16] M. Klein, D. Zur, D. Menzel, J. Schoenes, K. Doll, J. Röder, and F. Reinert, Evidence for Itineracy in the Anticipated Kondo Insulator FeSi: A Quantitative Determination of the Band Renormalization, Phys. Rev. Lett. **101**, 046406 (2008).

[17] M. Klein, D. Menzel, K. Doll, M. Neef, D. Zur, I. Jursic, J. Schoenes, and F. Reinert, Photoemission spectroscopy across the semiconductor-to-metal transition in FeSi, New J. Phys. **11**, 023026 (2009).

[18] N. Manyala, Y. Sidis, J. F. DiTusa, G. Aeppli, D. P. Young, and Z. Fisk, Magnetoresistance from quantum interference effects in ferromagnets, Nature (London) **404**, 581 (2000).

[19] E. Bauer, A. Galatanu, R. Hauser, Ch. Reichl, G. Wiesinger, G. Zaussinger, M. Galli, and F. Marabelli, Evolution of a metallic and magnetic state in (Fe,Mn)Si and Fe(Si,Ge), J. Magn. Magn. Mater. **177**, 1401 (1998).

[20] B. C. Sales, E. C. Jones, B. C. Chakoumakos, J. A. Fernandez-Baca, H. E. Harmon, J. W. Sharp, and E. H. Volckmann, Magnetic, transport, and structural properties of $Fe_{1-x}Ir_xSi$, Phys. Rev. B **50**, 8207 (1994).

[21] B. C. Sales, O. Delaire, M. A. McGuire, and A. F. May, Thermoelectric properties of Co-, Ir- and Os-doped FeSi alloys: Evidence for strong electron-phonon coupling, Phys. Rev. B **83**, 125209 (2011).

[22] Ch. Reichl, G. Wiesinger, G. Zaussinger, E. Bauer, M. Galli, and F. Marabelli, On electronic and pressure response of $FeSi_{1-x}Ge_x$, Physica B **259**, 866 (1999).

[23] R. Pelzer, L. Naber, A. Galatanu, H. Sassik, and E. Bauer, Pressure response of $Fe_{1-x}Si_{1+x}$, $-0.003 \leqslant x \leqslant 0.025$, J. Magn. Magn. Mater. **226-230**, 227 (2001).

[24] A. Mani, A. Bharathi, and Y. Hariharan, Pressure-induced insulator-metal transition of localized states in $FeSi_{1-x}Ge_x$, Phys. Rev. B **63**, 115103 (2001).

[25] L. Pauling and A. M. Soldate, The nature of the bonds in the iron silicide, FeSi, and related crystals, Acta Crystallogr. **1**, 212 (1948).

[26] I. G. Wood, W. I.E. David, S. Hull, and G. D. Price, A high-pressure study of ε-FeSi, between 0 and 8.5 GPa, by time-of-flight neutron powder diffraction, J. Appl. Crystallogr. **29**, 215 (1996).

[27] B. Buschinger, C. Geibel, F. Steglich, D. Mandrus, D. P. Young, J. L. Sarrao, and Z. Fisk, Transport properties of FeSi, Physica B: **230**, 784 (1997).

[28] J. DiTusa, K. Friemelt, E. Bucher, G. Aeppli, and A. P. Ramirez, Heavy fermion metal-Kondo insulator transition in $FeSi_{1-x}Al_x$, Phys. Rev. B **58**, 10288 (1998).

[29] See Supplemental Material at http://link.aps.org/supplemental/10.1103/PhysRevB.100.155118, which also includes details on sample characterization involving Refs. [30,31] amongst others also cited in the main text. There are also two further series of

resistivity measurements at pressure on related FeSi samples in addition to what is in the main text.

[30] M. Fanciulli, A. Zenkevich, I. Wenneker, A. Svane, N. E. Christensen, and G. Weyer, Electric-field gradient at the Fe nucleus in ε-FeSi, Phys. Rev. B **54**, 15985 (1996).

[31] G. K. Wertheim, J. H Wernick, and D. N. E. Buchanan. Mössbauer effect in $Co_{1-x}Fe_xSi$, J. Appl Phys. **37**, 3333 (1966).

[32] M. K. Forthaus, G. R. Hearne, N. Manyala, O. Heyer, R. A. Brand, D. I. Khomskii, T. Lorenz, and M. M. Abd-Elmeguid, Pressure-induced quantum phase transition in $Fe_{1-x}Co_xSi$ ($x = 0.1, 0.2$), Phys. Rev. B **83**, 085101 (2011).

[33] A. D. Chijioke, W. J. Nellis, A. Soldatov, and I. F. Silvera, The ruby pressure standard to 150 GPa, J. Appl. Phys. **98**, 114905 (2005).

[34] S. Klotz, J.-C. Chervin, P. Munsch, and G. L. Marchand, Hydrostatic limits of 11 pressure transmitting media, J. Phys. D: Appl. Phys. **42**, 075413 (2009).

[35] G. R. Stewart, Non-Fermi liquid behavior in d- and f-electron metals, Rev. Mod. Phys. **73**, 797 (2001).

[36] A. Rosch, Interplay of Disorder and Spin Fluctuations in the Resistivity near a Quantum Critical Point, Phys. Rev. Lett. **82**, 4280 (1999).

[37] F. D. Murnaghan, The compressibility of media under extreme pressures, Proc. Natl. Acad. Sci. USA **30**, 244 (1944).

[38] J.-F. Lin, A. J. Campbell, D. L. Heinz, and G. Shen, Static compression of iron-silicon alloys: Implications for silicon in the Earth's core, J. Geophys. Res. **108**, 11 (2003).

[39] T. Jarlborg, ε-FeSi: A material sensitive to thermal disorder, Phys. Lett. A **236**, 143 (1997).

[40] T. Jarlborg, Electronic structure and properties of pure and doped ε-FeSi from *ab initio* local-density theory, Phys. Rev. B **59**, 15002 (1999).

[41] Y. Onose, N. Takeshita, C. Terakura, H. Takagi, and Y. Tokura, Doping dependence of transport properties in $Fe_{1-x}Co_xSi$, Phys. Rev. B **72**, 224431 (2005).

[42] K. Ishimoto, M. Ohashi, H. Yamauchi, and Y. Yamaguchi, Itinerant electron ferromagnetism in $Fe_{1-x}Co_xSi$ studied by polarized neutron diffraction, J. Phys. Soc. Jpn. **61**, 2503 (1992).